Temperature dependence of the superfluid density in a noncentrosymmetric superconductor

N. Hayashi,[1] K. Wakabayashi,[1,2] P. A. Frigeri,[1] and M. Sigrist[1]
[1]*Institut für Theoretische Physik, ETH-Hönggerberg, CH-8093 Zürich, Switzerland*
[2]*Department of Quantum Matter Science, Graduate School of Advanced Sciences of Matter (ADSM), Hiroshima University, Higashi-Hiroshima 739-8530, Japan*
(Received 25 August 2005; revised manuscript received 20 October 2005; published 19 January 2006)

For a noncentrosymmetric superconductor such as $CePt_3Si$, we consider a Cooper pairing model with a two-component order parameter composed of spin-singlet and spin-triplet pairing components. We calculate the superfluid density tensor in the clean limit on the basis of the quasiclassical theory of superconductivity. We demonstrate that such a pairing model accounts for an experimentally observed feature of the temperature dependence of the London penetration depth in $CePt_3Si$, i.e., line-node-gap behavior at low temperatures.

DOI: 10.1103/PhysRevB.73.024504 PACS number(s): 74.20.Rp, 74.70.Tx, 74.25.Bt

I. INTRODUCTION

Much attention has been focused on the superconductivity in systems without inversion symmetry (e.g, Refs. 1–6, and references therein). Recently, $CePt_3Si$ was found to be a heavy fermion superconductor without inversion symmetry in the crystal structure.[7–10] This motivates more detailed studies of the superconductivity in noncentrosymmetric systems. The lack of an inversion center in the crystal lattice induces antisymmetric spin-orbit coupling[11,12] responsible for a mixing of spin-singlet and spin-triplet Cooper pairings.[2] In $CePt_3Si$, this mixing of the pairing channels with different parity may result in unusual properties of experimentally observed quantities such as a very high upper critical field H_{c2} which exceeds the paramagnetic limit,[7–10,13] and the simultaneous appearance of a coherence peak feature in the NMR relaxation rate T_1^{-1} and low-temperature power-law behavior suggesting line nodes in the quasiparticle gap[8–10,14–16] (see also Ref. 17). The presence of line nodes in the gap of $CePt_3Si$ is also indicated by measurements of the thermal conductivity[18] and the London penetration depth.[10,19]

In $CePt_3Si$, the superconductivity coexists with an antiferromagnetic phase[7–10,14–16,20,21] (see also Ref. 22). Generally one may have to include this aspect when the low-temperature thermodynamics is analyzed in this material. The London penetration depth, however, which is entirely connected with the superfluid density, contains exclusively the information on the superconductivity and provides for this reason a very suitable probe of the low-energy spectrum of the quasiparticles associated with the superconducting gap topology. Experimental measurements of the London penetration depth on polycrystalline and powder samples are reported in Refs. 10 and 19. We note that $CePt_3Si$ is an extreme type-II superconductor with the Ginzburg-Landau parameter $\kappa \simeq 140$,[7,10] and the nonlocal effect can be safely neglected.

For a noncentrosymmetric superconductor such as $CePt_3Si$, we will consider a Cooper pairing model with an order parameter consisting of spin-singlet and spin-triplet pairing components. Based on the same pairing model, we previously investigated the nuclear spin-lattice relaxation rate to explain peculiarities observed in T_1^{-1}.[23–25] In this paper, we calculate the superfluid density and demonstrate that this pairing model simultaneously gives an explanation of the power-law temperature dependence of the penetration depth at low temperatures in $CePt_3Si$.

This paper is organized as follows. In Sec. II, we describe the electronic structure of the system without inversion symmetry and our pairing model. In Sec. III, the equations for calculating the superfluid density are formulated. The numerical results are shown in Sec. IV. The summary is given in Sec. V. In the Appendix, we describe the derivation of the quasiclassical Green functions used to compute the superfluid density for the present pairing model.

II. SYSTEM WITHOUT INVERSION SYMMETRY

We base our analysis on a system considered in Ref. 3, where the lack of inversion symmetry is incorporated through the antisymmetric Rashba-type spin-orbit coupling[3,26–29]

$$\sum_{\mathbf{k},\eta,\eta'} \alpha \mathbf{g}_k \cdot \hat{\boldsymbol{\sigma}}_{\eta\eta'} c^\dagger_{\mathbf{k}\eta} c_{\mathbf{k}\eta'}, \tag{1}$$

with

$$\mathbf{g}_k = \sqrt{\frac{3}{2}} \frac{1}{k_F} (-k_y, k_x, 0). \tag{2}$$

Here, $\hat{\boldsymbol{\sigma}} = (\hat{\sigma}_x, \hat{\sigma}_y, \hat{\sigma}_z)$ is the vector consisting of the Pauli matrices, $c^\dagger_{\mathbf{k}\eta}$ ($c_{\mathbf{k}\eta}$) is the creation (annihilation) operator for the quasiparticle state with momentum $\mathbf{k}$ and spin η. We use units in which $\hbar = k_B = 1$. α (>0) denotes the strength of the spin-orbit coupling. The antisymmetric vector $\mathbf{g}_k$ ($\mathbf{g}_{-k} = -\mathbf{g}_k$) is determined by symmetry arguments and is normalized as $\langle \mathbf{g}_k^2 \rangle_0 = 1$.[3,26] k_F is the Fermi wave number and the brackets $\langle \ldots \rangle_0$ denote the average over the Fermi surface in the case of $\alpha = 0$.

Generally we may classify the basic pairing states for a superconductor of given crystal symmetry, distinguishing the spin-singlet and spin-triplet states.[3,5] A general argument by Anderson[30] shows that the inversion symmetry is a key element for the realization of spin-triplet pairing states. Hence,

the lack of inversion symmetry as in $CePt_3Si$ may be detrimental for spin-triplet pairing states. In other words, the presence of the antisymmetric spin-orbit coupling would suppress spin-triplet pairing. However, it has been shown by Frigeri *et al.*[3] that the antisymmetric spin-orbit coupling is not destructive to the special spin-triplet state with the **d** vector parallel to $\mathbf{g}_k$ ($\mathbf{d}_k \| \mathbf{g}_k$). Therefore, referring to $\mathbf{g}_k$ given in Eq. (2), we adopt the *p*-wave pairing state with parallel **d** vector, $\mathbf{d}_k = \Delta(-\tilde{k}_y, \tilde{k}_x, 0)$.[31] Here, the unit vector $\tilde{\mathbf{k}} = (\tilde{k}_x, \tilde{k}_y, \tilde{k}_z) = (\cos\phi \sin\theta, \sin\phi \sin\theta, \cos\theta)$. A further effect of the antisymmetric spin-orbit coupling is the mixing of spin-singlet and spin-triplet pairing components.[2] Interestingly, only the *s*-wave spin-singlet pairing state (belonging to A_{1g} representation of crystal point group) mixes with the above *p*-wave spin-triplet pairing state (for example, *d*-wave states cannot mix with this *p*-wave state because of symmetry).[29,32]

This parity-mixed pairing state is expressed by the order parameter,

$$\hat{\Delta}(\mathbf{r}, \tilde{\mathbf{k}}) = [\Psi(\mathbf{r})\hat{\sigma}_0 + \mathbf{d}_k(\mathbf{r}) \cdot \hat{\boldsymbol{\sigma}}] i\hat{\sigma}_y$$
$$= [\Psi(\mathbf{r})\hat{\sigma}_0 + \Delta(\mathbf{r})(-\tilde{k}_y\hat{\sigma}_x + \tilde{k}_x\hat{\sigma}_y)] i\hat{\sigma}_y, \quad (3)$$

with the spin-singlet *s*-wave component $\Psi(\mathbf{r})$ and the **d** vector $\mathbf{d}_k(\mathbf{r}) = \Delta(\mathbf{r})(-\tilde{k}_y, \tilde{k}_x, 0)$. Here, the vector **r** indicates the real-space coordinates, and $\hat{\sigma}_0$ is the unit matrix in the spin space. While this spin-triplet part alone has point nodes, the pairing state of Eq. (3) can possess line nodes in a gap as a result of the combination with the *s*-wave component.[23,29,33] In this paper, we choose the isotropic *s*-wave pairing as Ψ for simplicity.

III. QUASICLASSICAL FORMULATION

We will calculate the superfluid density on the basis of the quasiclassical theory of superconductivity.[34–36] Following the spirit of the theory,[36] in this study we assume $|\Psi|, |\Delta|, \alpha \ll \varepsilon_F$ (ε_F is the Fermi energy). We consider the quasiclassical Green function $\check{g}$ which has the matrix elements in Nambu (particle-hole) space as

$$\check{g}(\mathbf{r}, \tilde{\mathbf{k}}, i\omega_n) = -i\pi \begin{pmatrix} \hat{g} & i\hat{f} \\ -i\hat{\bar{f}} & -\hat{\bar{g}} \end{pmatrix}, \quad (4)$$

where $\omega_n = \pi T(2n+1)$ is the Matsubara frequency (with the temperature T and the integer n). Throughout the paper, a "hat" ($\hat{\bullet}$) denotes the 2×2 matrix in the spin space, and a "check" ($\check{\bullet}$) denotes the 4×4 matrix composed of the 2×2 Nambu space and the 2×2 spin space.

The Eilenberger equation which includes the spin-orbit coupling term is given as[23,37–41]

$$i\mathbf{v}_F(s) \cdot \boldsymbol{\nabla}\check{g} + [i\omega_n\check{\tau}_3 - \alpha\check{\mathbf{g}}_k \cdot \check{\mathbf{S}} - \check{\Delta}, \check{g}] = 0, \quad (5)$$

with

$$\check{\tau}_3 = \begin{pmatrix} \hat{\sigma}_0 & 0 \\ 0 & -\hat{\sigma}_0 \end{pmatrix}, \quad (6)$$

$$\check{\mathbf{S}} = \begin{pmatrix} \hat{\boldsymbol{\sigma}} & 0 \\ 0 & \hat{\boldsymbol{\sigma}}^{tr} \end{pmatrix}, \quad \hat{\boldsymbol{\sigma}}^{tr} = -\hat{\sigma}_y\hat{\boldsymbol{\sigma}}\hat{\sigma}_y, \quad (7)$$

$$\check{\mathbf{g}}_k = \begin{pmatrix} \mathbf{g}_k\hat{\sigma}_0 & 0 \\ 0 & \mathbf{g}_{-k}\hat{\sigma}_0 \end{pmatrix} = \begin{pmatrix} \mathbf{g}_k\hat{\sigma}_0 & 0 \\ 0 & -\mathbf{g}_k\hat{\sigma}_0 \end{pmatrix}, \quad (8)$$

$$\mathbf{g}_k = \sqrt{\frac{3}{2}}(-\tilde{k}_y, \tilde{k}_x, 0), \quad (9)$$

$$\check{\Delta} = \begin{pmatrix} 0 & \hat{\Delta} \\ -\hat{\Delta}^\dagger & 0 \end{pmatrix}. \quad (10)$$

Here, $\mathbf{v}_F(s)$ is the Fermi velocity, the variable s indicates the position on the Fermi surfaces, and the commutator $[\check{a}, \check{b}] = \check{a}\check{b} - \check{b}\check{a}$. The Eilenberger equation is supplemented by the normalization condition[34,37]

$$\check{g}^2 = -\pi^2\check{1}, \quad (11)$$

where $\check{1}$ is the 4×4 unit matrix. Because $CePt_3Si$ is a clean superconductor,[7,10] we neglect the impurity effect.

To obtain an expression for the superfluid density, we follow the procedure developed by Choi *et al.*[42–46] We consider a system in which a uniform supercurrent flows with the velocity $\mathbf{v}_s$, and the gap function (3) has the **r** dependence as[42–46]

$$\hat{\Delta}(\mathbf{r}, \tilde{\mathbf{k}}) = \hat{\Delta}'(\tilde{\mathbf{k}}) e^{i2M\mathbf{v}_s \cdot \mathbf{r}}$$
$$= [\Psi\hat{\sigma}_0 + \Delta(-\tilde{k}_y\hat{\sigma}_x + \tilde{k}_x\hat{\sigma}_y)] i\hat{\sigma}_y e^{i2M\mathbf{v}_s \cdot \mathbf{r}}, \quad (12)$$

and accordingly

$$\Psi(\mathbf{r}) = \Psi e^{i2M\mathbf{v}_s \cdot \mathbf{r}}, \quad \Delta(\mathbf{r}) = \Delta e^{i2M\mathbf{v}_s \cdot \mathbf{r}}. \quad (13)$$

The bare electron mass is denoted by M. The matrix elements of the Green function (4) are expressed as

$$\hat{g}(\mathbf{r}, \tilde{\mathbf{k}}, i\omega_n) = \hat{g}'(\tilde{\mathbf{k}}, i\omega_n), \quad (14a)$$

$$\hat{f}(\mathbf{r}, \tilde{\mathbf{k}}, i\omega_n) = \hat{f}'(\tilde{\mathbf{k}}, i\omega_n) e^{i2M\mathbf{v}_s \cdot \mathbf{r}}, \quad (14b)$$

$$\hat{\bar{f}}(\mathbf{r}, \tilde{\mathbf{k}}, i\omega_n) = \hat{\bar{f}}'(\tilde{\mathbf{k}}, i\omega_n) e^{-i2M\mathbf{v}_s \cdot \mathbf{r}}, \quad (14c)$$

$$\hat{\bar{g}}(\mathbf{r}, \tilde{\mathbf{k}}, i\omega_n) = \hat{\bar{g}}'(\tilde{\mathbf{k}}, i\omega_n). \quad (14d)$$

The Eilenberger equation (5) is rewritten in a form without the **r** dependence as

$$[i(\omega_n + q)\check{\tau}_3 - \alpha\check{\mathbf{g}}_k \cdot \check{\mathbf{S}} - \check{\Delta}', \check{g}'] = 0, \quad (15)$$

with

$$q = iM\mathbf{v}_F(s) \cdot \mathbf{v}_s, \quad (16)$$

$$\check{g}' = -i\pi \begin{pmatrix} \hat{g}' & i\hat{f}' \\ -i\hat{\bar{f}}' & -\hat{\bar{g}}' \end{pmatrix}, \quad (17)$$

$$\check{\Delta}' = \begin{pmatrix} 0 & \hat{\Delta}' \\ -\hat{\Delta}'^{\dagger} & 0 \end{pmatrix}. \tag{18}$$

We obtain the following Green functions from the Eilenberger equation and the normalization condition (see Appendix),

$$\hat{g}' = g_{\mathrm{I}}\hat{\sigma}_{\mathrm{I}} + g_{\mathrm{II}}\hat{\sigma}_{\mathrm{II}}, \tag{19a}$$

$$\hat{f}' = (f_{\mathrm{I}}\hat{\sigma}_{\mathrm{I}} + f_{\mathrm{II}}\hat{\sigma}_{\mathrm{II}})i\hat{\sigma}_y, \tag{19b}$$

with the matrices $\hat{\sigma}_{\mathrm{I}}$ and $\hat{\sigma}_{\mathrm{II}}$ defined by[1,29,47]

$$\hat{\sigma}_{\mathrm{I,II}} = \frac{1}{2}(\hat{\sigma}_0 \pm \bar{\mathbf{g}}_k \cdot \hat{\boldsymbol{\sigma}}), \quad \bar{\mathbf{g}}_k = (-\bar{k}_y, \bar{k}_x, 0). \tag{20}$$

Here, $\bar{\mathbf{k}} = (\bar{k}_x, \bar{k}_y, 0) = (\cos\phi, \sin\phi, 0)$, and

$$g_{\mathrm{I}} = \frac{\omega_n + q}{B_{\mathrm{I}}}, \quad g_{\mathrm{II}} = \frac{\omega_n + q}{B_{\mathrm{II}}}, \tag{21a}$$

$$f_{\mathrm{I}} = \frac{\Psi + \Delta \sin\theta}{B_{\mathrm{I}}}, \quad f_{\mathrm{II}} = \frac{\Psi - \Delta \sin\theta}{B_{\mathrm{II}}}. \tag{21b}$$

The denominators B_{I} and B_{II} are given as

$$B_{\mathrm{I}} = \pm\sqrt{(\omega_n + q)^2 + |\Psi + \Delta \sin\theta|^2}, \tag{22a}$$

$$B_{\mathrm{II}} = \pm\sqrt{(\omega_n + q)^2 + |\Psi - \Delta \sin\theta|^2}, \tag{22b}$$

and the signs in front of the square root are determined by the conditions

$$\mathrm{sgn}(\mathrm{Re}\{g_{\mathrm{I}}\}) = \mathrm{sgn}(\mathrm{Re}\{\omega_n\}), \tag{23a}$$

$$\mathrm{sgn}(\mathrm{Re}\{g_{\mathrm{II}}\}) = \mathrm{sgn}(\mathrm{Re}\{\omega_n\}). \tag{23b}$$

The Green functions labeled by the indices I and II belong to the two distinct Fermi surfaces which are split by the lifting of the spin degeneracy due to the spin-orbit coupling. The densities of states on those two Fermi surfaces are different from each other in general. We define the density of states (the Fermi velocity) as $N_{\mathrm{I,II}}$ ($\mathbf{v}_{\mathrm{I,II}}$) on the Fermi surfaces I and II. We also define a parameter δ ($-1 < \delta < 1$) which parametrizes the difference in the density of states,

$$\delta = \frac{N_{\mathrm{I}} - N_{\mathrm{II}}}{2N_0}, \tag{24}$$

where $2N_0 = N_{\mathrm{I}} + N_{\mathrm{II}}$. We consider δ as a parameter independent of α.

The supercurrent $\mathbf{J}$ is composed of the regular part, $-i\pi\hat{g}$, of the Green function in Eq. (4).[36] $\mathbf{J}$ is expressed by

$$\mathbf{J} = T\sum_{\omega_n} \int ds N_{\mathrm{F}}(s)\mathbf{v}_{\mathrm{F}}(s)\mathrm{tr}[\hat{\sigma}_0(-i\pi\hat{g})]$$

$$= \frac{\pi T}{i}\sum_{\omega_n} [N_{\mathrm{I}}\langle \mathbf{v}_{\mathrm{I}} g_{\mathrm{I}}\rangle + N_{\mathrm{II}}\langle \mathbf{v}_{\mathrm{II}} g_{\mathrm{II}}\rangle], \tag{25}$$

where $N_{\mathrm{F}}(s)$ is the density of states at the position s on the Fermi surfaces, "tr" means the trace in the spin space, and the brackets $\langle\ldots\rangle$ denote the average over each Fermi surface. In Eq. (25), we have referred to Eqs. (14a) and (19a). In order to calculate the superfluid density tensor ρ_{ij} ($J_i = \rho_{ij} v_{sj}$), we expand $g_{\mathrm{I,II}}$ in Eq. (21a) up to first order in $\mathbf{v}_s$ (or q), and substitute them into Eq. (25). The expression for ρ_{ij} is then obtained as[48]

$$\rho_{ij} = M\pi T\sum_{\omega_n} \left[N_{\mathrm{I}} \left\langle \frac{v_{\mathrm{I}i} v_{\mathrm{I}j} |\Psi + \Delta \sin\theta|^2}{(\omega_n^2 + |\Psi + \Delta \sin\theta|^2)^{3/2}} \right\rangle + N_{\mathrm{II}} \left\langle \frac{v_{\mathrm{II}i} v_{\mathrm{II}j} |\Psi - \Delta \sin\theta|^2}{(\omega_n^2 + |\Psi - \Delta \sin\theta|^2)^{3/2}} \right\rangle \right]. \tag{26}$$

Now, to compute the superfluid density tensor ρ_{ij} in Eq. (26), we need to assume a model of the Fermi surfaces. For the shape of the Fermi surfaces, we adopt the spherical Fermi surface for simplicity, and thus $\mathbf{v}_{\mathrm{I,II}} = v_{\mathrm{I,II}}\tilde{\mathbf{k}} = v_{\mathrm{I,II}}$ ($\cos\phi \sin\theta, \sin\phi \sin\theta, \cos\theta$) and the Fermi-surface average $\langle\ldots\rangle = (1/4\pi)\int_0^{2\pi} d\phi \int_0^{\pi} d\theta \sin\theta \ldots$.[49] This spherical approximation is justified for $CePt_3Si$, since measurements of H_{c2} give evidence for a nearly isotropic mass tensor.[7,13] We furthermore set the two Fermi velocities equal,[50]

$$v_{\mathrm{I}} = v_{\mathrm{II}} \equiv v. \tag{27}$$

From Eq. (26), the components of the superfluid density tensor are obtained as

$$\rho_{xx} = (Mv^2 N_0) 2\pi T \sum_{\omega_n > 0} \times \frac{1}{2}\left[C_{\mathrm{I}}(\delta) \int_0^{\pi} \frac{d\theta}{2} \frac{|\Psi + \Delta \sin\theta|^2 \sin^3\theta}{(\omega_n^2 + |\Psi + \Delta \sin\theta|^2)^{3/2}} + C_{\mathrm{II}}(\delta) \int_0^{\pi} \frac{d\theta}{2} \frac{|\Psi - \Delta \sin\theta|^2 \sin^3\theta}{(\omega_n^2 + |\Psi - \Delta \sin\theta|^2)^{3/2}} \right], \tag{28}$$

$$\rho_{zz} = (Mv^2 N_0) 2\pi T \sum_{\omega_n > 0} \times \left[C_{\mathrm{I}}(\delta) \int_0^{\pi} \frac{d\theta}{2} \frac{|\Psi + \Delta \sin\theta|^2 \sin\theta \cos^2\theta}{(\omega_n^2 + |\Psi + \Delta \sin\theta|^2)^{3/2}} + C_{\mathrm{II}}(\delta) \int_0^{\pi} \frac{d\theta}{2} \frac{|\Psi - \Delta \sin\theta|^2 \sin\theta \cos^2\theta}{(\omega_n^2 + |\Psi - \Delta \sin\theta|^2)^{3/2}} \right], \tag{29}$$

$\rho_{xy} = \rho_{yx} = 0$, $\rho_{zx} = \rho_{xz} = \rho_{zy} = \rho_{yz} = 0$, and $\rho_{yy} = \rho_{xx}$. Here, the weighting factors $C_{\mathrm{I,II}}$ in the case of the model of Eq. (27) are given as

$$C_{\mathrm{I}}(\delta) = 1 + \delta, \quad C_{\mathrm{II}}(\delta) = 1 - \delta. \tag{30}$$

At zero temperature,

$$\rho \equiv \rho_{xx}(T=0) = \rho_{zz}(T=0) = \frac{2}{3} Mv^2 N_0, \tag{31}$$

where we have utilized a formula for an arbitrary function F, $\lim_{T\to 0} 2\pi T \Sigma_{\omega_n} F(\omega_n) = \int d\omega F(\omega)$.

The gap equations for the order parameters Ψ and Δ are given by[29,48]

$$\Psi = \pi T \sum_{|\omega_n|<\omega_c} [\lambda_s \langle f_+ \rangle + \delta\lambda_s \langle f_- \rangle + \lambda_m \langle \sin\theta f_- \rangle + \delta\lambda_m \langle \sin\theta f_+ \rangle], \tag{32}$$

$$\Delta = \pi T \sum_{|\omega_n|<\omega_c} [\lambda_t \langle \sin\theta f_- \rangle + \delta\lambda_t \langle \sin\theta f_+ \rangle + \lambda_m \langle f_+ \rangle + \delta\lambda_m \langle f_- \rangle], \tag{33}$$

where

$$f_\pm = \frac{f_{\mathrm{I}} \pm f_{\mathrm{II}}}{2}, \tag{34}$$

and ω_c is the cutoff energy. The coupling constants λ_s and λ_t result from the pairing interaction within each spin channel (s: singlet, t: triplet). λ_m appears as a scattering of Cooper pairs between the two channels, which is allowed in a system without inversion symmetry.[29]

In the limit $T \to T_c$ (T_c is the superconducting critical temperature), the linearized gap equations allow us to determine λ_s and λ_t by

$$\lambda_s = \left[\frac{1}{w} - \lambda_m\left(\frac{2}{3\nu} + \frac{\pi\delta}{4}\right)\right] \Bigg/ \left(1 + \frac{\pi\delta}{4\nu}\right), \tag{35}$$

$$\lambda_t = \left[\frac{1}{w} - \lambda_m\left(\nu + \frac{\pi\delta}{4}\right)\right] \Bigg/ \left(\frac{2}{3} + \frac{\pi\delta\nu}{4}\right), \tag{36}$$

$$w = \ln\left(\frac{T}{T_c}\right) + \sum_{0\le n<(\omega_c/\pi T-1)/2} \frac{2}{2n+1}, \tag{37}$$

$$\nu = \left.\frac{\Psi}{\Delta}\right|_{T\to T_c-0^+}, \tag{38}$$

when the parameters λ_m and ν are given.

IV. NUMERICAL RESULTS

In this section, we will show the numerically evaluated results for the superfluid densities ρ_{xx} and ρ_{zz}. To calculate them in Eqs. (28) and (29), we need the temperature dependence of the order parameters Ψ and Δ. We will use the order parameters obtained from the gap equations [Eqs. (32) and (33)] for the parameters $\omega_c = 100T_c$ and $\lambda_m = 0.2$. This is a representative set of parameters. Different choices would not lead to qualitatively different results as long as the gap topology is not altered. We have calculated the superfluid densities also for $\lambda_m = 0.1$ and obtained qualitatively the same results.

The Green functions in Eq. (A18) are substituted into the gap equations. When solving the gap equations, Δ is fixed to be real without loss of generality, resulting in a real Ψ as well.[29] Referring to Eq. (21b), we notice that the superconducting gaps are $|\Psi + \Delta \sin\theta|$ and $|\Psi - \Delta \sin\theta|$ on the Fermi surfaces I and II, respectively. Such a gap structure can lead to line nodes on either Fermi surface I or II (as shown in Fig. 1).[23,29,33] When the signs of Ψ and Δ are reverse to (same as) each other, gap nodes appear on the Fermi surface I (II). The relative sign is controlled by the parameters λ_m, δ, and ν in the present formulation. In this paper, we choose such parameters as $\Psi > 0$ and $\Delta > 0$, so that gap nodes ($|\Psi - \Delta \sin\theta| = 0$) appear on the Fermi surface II (see Fig. 1). Under this circumstance, we can obtain stable order parameters Ψ and Δ when the difference in the density of states δ defined in Eq. (24) is set as $\delta \gtrsim -0.2$ for $\lambda_m = 0.1$ and 0.2. For $\delta \gtrsim -0.2$, stable Ψ and Δ are obtained when the singlet-to-triplet components ratio ν defined in Eq. (38) is set as $\nu \gtrsim 0.3$ ($\lambda_m = 0.1$) and $\nu \gtrsim 0.5$ ($\lambda_m = 0.2$).

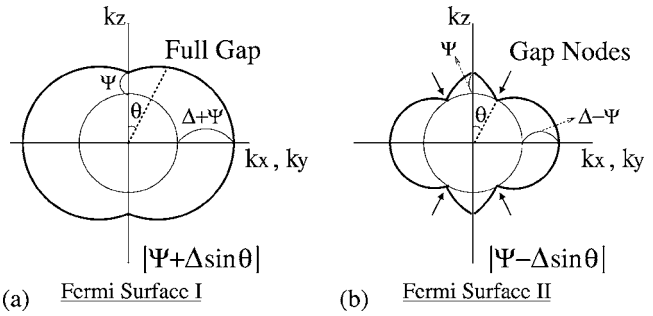

FIG. 1. Schematic figures of the gap structure on the Fermi surfaces. (a) On Fermi surface I, the gap is $|\Psi + \Delta \sin\theta|$. (b) On Fermi surface II, the gap is $|\Psi - \Delta \sin\theta|$. In these figures, it is assumed that both Ψ and Δ are real and positive, and $\Psi < \Delta$.

In Fig. 2, we show in a low-temperature region the reciprocal square root of the superfluid densities $1/\sqrt{\rho_{xx}(T)}$ and $1/\sqrt{\rho_{zz}(T)}$, which correspond to the London penetration depth $\lambda_L(T)$. We set here the parameter $\nu = 0.6$, for which the gap nodes are line nodes on the Fermi surface II.[23] Indeed, the data exhibit the T-linear behavior at low temperatures, indicating the existence of line nodes. For comparison, we also plot in Fig. 2 the same quantities calculated for a point-node gap (dotted line), which is contrasting well with the line-node-gap behavior. The present results explain the experimentally observed T-linear behavior of $\lambda_L(T)$ in $CePt_3Si$.[10,19] We note here that $CePt_3Si$ is an extreme type-II superconductor[7,10] and nonlocal effects can be neglected.

Concerning the dependence on δ the difference in the density of states [Eq. (24)], we notice in Fig. 2 that the smaller δ ($-1 < \delta < 1$), the stronger temperature dependence appears. Note the nearly temperature-independent behavior of the state with point nodes (dotted line) at low temperatures corresponding to a T^3 behavior. This indicates weaker contributions of low-energy quasiparticles. For the identical Fermi velocities on the two Fermi surfaces, the smaller δ ($-1 < \delta < 1$) leads to a smaller weighting factor $C_{\mathrm{I}} = 1 + \delta$ and a larger $C_{\mathrm{II}} = 1 - \delta$. Therefore, with decreasing δ, to the superfluid densities the contribution of the fully gapped Fermi surface I shrinks with the decreasing weighting factor $C_{\mathrm{I}} = 1 + \delta$. On the other hand, the contribution of the Fermi surface II with the gap nodes increases because of the growing weighting factor $C_{\mathrm{II}} = 1 - \delta$ and the effect of the line-node-gapped Fermi surface II is enhanced by decreasing δ (Fig. 2).

In Figs. 3 and 4, we show the superfluid densities $\rho_{xx}(T)$ and $\rho_{zz}(T)$ to see the overall temperature dependence. The quantities correspond to $1/\lambda_L^2(T)$. With decreasing δ (-1

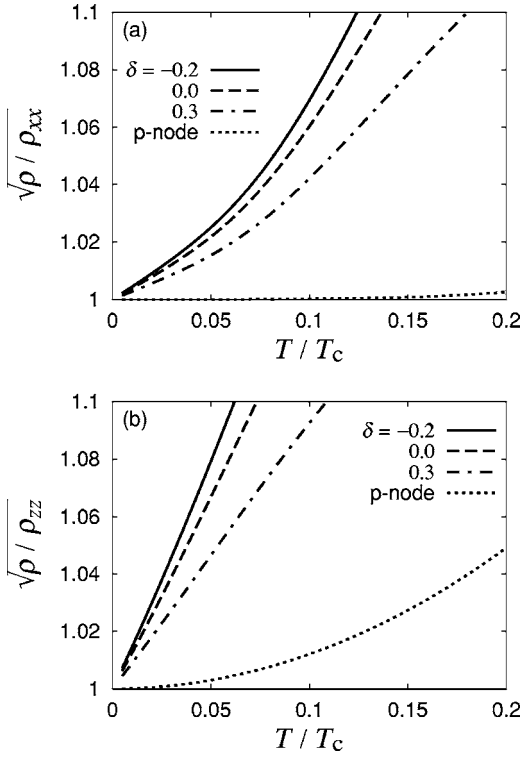

FIG. 2. Plots of the reciprocal square root of the superfluid densities vs temperature, $1/\sqrt{\rho_{xx}}$ (a) and $1/\sqrt{\rho_{zz}}$ (b), for several values of the difference in the density of states δ. The singlet-to-triplet components ratio ν is set as $\nu=0.6$. For comparison, dotted lines indicate those for a point-node gap, i.e., pure p-wave gap $|\Delta \sin\theta|$ $(\Psi=0)$.

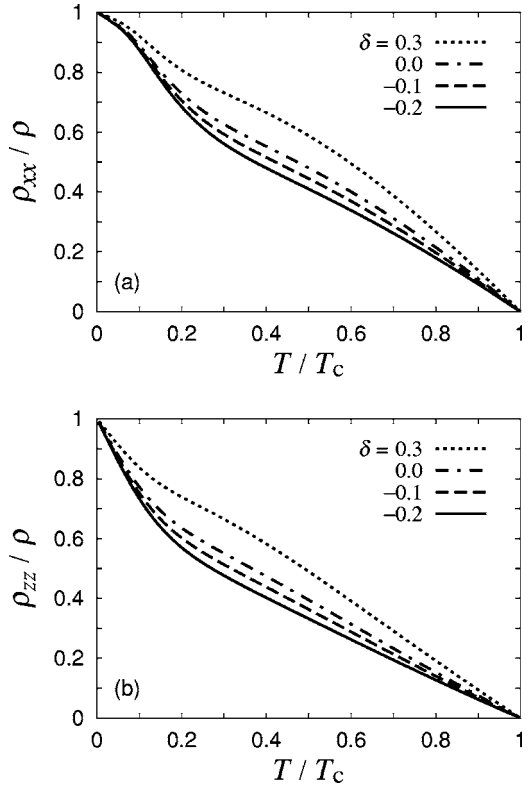

FIG. 3. The temperature dependence of the superfluid densities, ρ_{xx} (a) and ρ_{zz} (b), for several values of the difference in the density of states δ. The singlet-to-triplet components ratio ν is set as $\nu=0.6$.

$<\delta<1$) in Fig. 3, the curves deviate from an upper convex curve and become gradually upper concave curves, namely they deviate gradually from fully gapped s-wave behavior [i.e., $\rho_{ii}(T=0)-\rho_{ii}(T)\sim T^4$ in the s-wave case] because of the same reason mentioned above for the δ dependence in Fig. 2.

We show in Fig. 4 the dependence on the singlet-to-triplet components ratio ν [Eq. (38)]. With increasing ν in Fig. 4(a), the curvature of the upper concave curves of ρ_{xx} becomes larger. On the other hand, the ν dependence of ρ_{zz} is weaker than that of ρ_{xx}, as seen in Fig. 4(b). The quantity ρ_{xx} [Eq. (28)] senses the gap topology emphatically near the equator of the Fermi surfaces, while ρ_{zz} [Eq. (29)] senses it near the poles. For the singlet-to-triplet components ratio $\nu\gtrsim 0.5$, the places (or the angles θ) of gap nodes at which $|\Psi-\Delta \sin\theta|$ $=0$ (see Fig. 1) are sufficiently away from the poles, and gradually approach to the equator on the Fermi surface II with increasing ν. Therefore, ρ_{xx} (ρ_{zz}) is sensitive (not sensitive) to the change of ν for $\nu\gtrsim 0.5$ as seen in Fig. 4.

It is interesting to note the difference in the temperature dependence between ρ_{xx} and ρ_{zz}. In Fig. 5, we plot the ratios ρ_{zz}/ρ_{xx} as functions of the temperature for several values of ν. They exhibit a nonmonotonic temperature dependence in contrast with a monotonic one in the cases of the axial state (point-node gap at the poles) and the polar state (line-node gap at the equator) shown in Ref. 44.

We have so far shown the results obtained for the Fermi velocity model of Eq. (27) ($v_{\rm I}=v_{\rm II}$) and Eq. (30) [$C_{\rm I,II}(\delta)$ $=1\pm\delta$]. Alternatively, we have calculated the same quantities also for a different model: $v_{\rm I,II}\propto 1/N_{\rm I,II}$ [thus, $v_{\rm II}=v_{\rm I}(1+\delta)/(1-\delta)$ instead of Eq. (27)]. The weighting factors are accordingly $C_{\rm I}=1+\delta$ and $C_{\rm II}=(1+\delta)^2/(1-\delta)$ in this model, and $\rho\equiv\rho_{xx}(T=0)=\rho_{zz}(T=0)=(2Mv_{\rm I}^2N_0/3)(1+\delta)/(1-\delta)$. Because of these weighting factors $C_{\rm I}=1+\delta$ and $C_{\rm II}=(1+\delta)^2/(1-\delta)$, the larger δ $(-1<\delta<1)$, the more enhanced the contribution of the Fermi surface II becomes. It is an opposite dependence on δ as compared to the case of Eq. (30) [$C_{\rm I,II}(\delta)=1\pm\delta$]. The results for the superfluid densities are qualitatively similar to those obtained for the previous model of Eq. (27) ($v_{\rm I}=v_{\rm II}$) with replacing $\delta\rightarrow-\delta$ in Figs. 2–5. We plot, nevertheless, a result for an extreme case in Fig. 6, where we set $\nu=0.6$ and $\delta=0.9$. In this case, the superfluid densities are predominantly determined by the contribution of the Fermi surface II with gap nodes, owing to the extreme value $\delta=0.9$ and the resulting weighting factor $C_{\rm II}=(1+\delta)^2/(1-\delta)\gg C_{\rm I}=1+\delta$. It is noticed in Fig. 6 that the superfluid densities are suppressed at high temperatures. The temperature dependence of ρ_{xx} in the region $T\leqslant 0.3T_{\rm c}$ of Fig. 6 is well fitted into an experimental result for $1/\lambda_{\rm L}^2(T)$ in $CePt_3Si$,[19] and an unusually strong suppression of $1/\lambda_{\rm L}^2(T)$ at high temperatures[19] is somewhat similar to that of ρ_{zz} in Fig. 6. However, the difference in the density of states estimated from a band calculation for $CePt_3Si$ is $|\delta|\sim 0.25$–0.3.[4] Therefore, the strong suppression of $1/\lambda_{\rm L}^2(T)$ at high temperatures observed in $CePt_3Si$ (Ref. 19) remains to be accounted for at this moment.

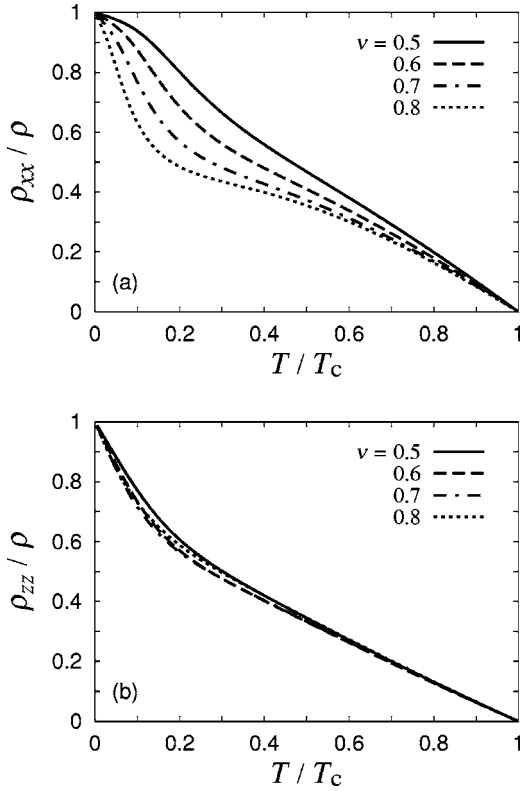

FIG. 4. The temperature dependence of the superfluid densities, ρ_{xx} (a) and ρ_{zz} (b), for several values of the singlet-to-triplet components ratio ν. The difference in the density of states is set as $\delta=-0.2$.

V. SUMMARY

We calculated the temperature dependence of the superfluid densities $\rho_{xx}(T)$ and $\rho_{zz}(T)$ for the noncentrosymmetric superconductor with the Rashba-type spin-orbit coupling represented by Eq. (2). We showed that the gap function of Eq. (3), which has the spin-singlet and spin-triplet pairing components, explains the line-node-gap temperature dependence of the experimentally observed $\lambda_L(T)$ in $CePt_3Si$.[10,19] While the low-temperature behavior ($T \lesssim 0.2T_c$) of $1/\lambda_L^2(T)$ can be reproduced qualitatively by that gap function, the high-temperature one still remains to be accounted for.

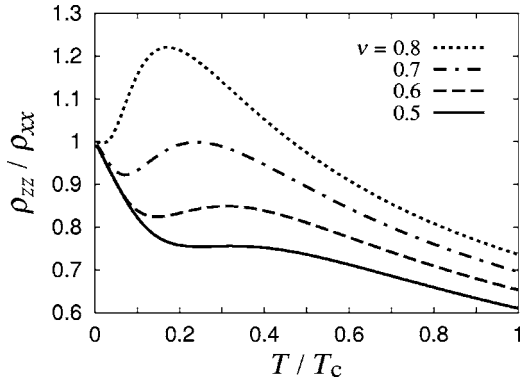

FIG. 5. Plots of the ratio ρ_{zz}/ρ_{xx} vs temperature for several values of the singlet-to-triplet components ratio ν. The difference in the density of states is set as $\delta=-0.2$.

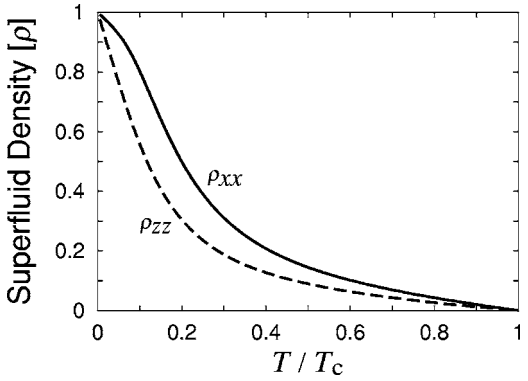

FIG. 6. The temperature dependence of the superfluid densities ρ_{xx} and ρ_{zz} for the Fermi velocity model, $v_{I,II} \propto 1/N_{I,II}$. $\nu=0.6$ and $\delta=0.9$.

The detailed information on the Fermi surfaces in the actual material $CePt_3Si$ is not available so far.[51] The main difficulty here lies in the fact that this material is a heavy fermion system with strongly renormalized carriers. If the Fermi velocity on the Fermi surface with gap nodes (on the Fermi surface II in our assumption) is sufficiently large in the case of the model $v_{I,II} \propto 1/N_{I,II}$ (otherwise, if $N_{II} \gg N_I$ in the case of $v_I \simeq v_{II}$), the anomalously strong suppression of $1/\lambda_L^2(T)$ observed experimentally at high temperatures[19] may be explained as in Fig. 6 (where $C_{II} \gg C_I$). Such an assumption seems not unreasonable in view of the large renormalization factors for the effective mass suggested from thermodynamic measurements. On the other hand, the London penetration depth was not measured on a single crystal, but on polycrystalline and powder samples,[10,19] to which the anomalous behavior at high temperatures could be attributed. We also note that the superconducting transition around T_c is rather broad in $CePt_3Si$ at least at this moment.[52] Thus, an unusual behavior of the superconducting phase close to T_c may also play a role in the T dependence of $1/\lambda_L^2(T)$. In any case, further experimental studies (e.g., experimental measurements on a single crystal) and theoretical studies using more information on the Fermi surfaces involved in superconductivity are needed in the future to accomplish a detailed fitting. It would also be important to experimentally test $CePt_3Si$ for the intriguing nonmonotonic temperature dependence of ρ_{zz}/ρ_{xx} (see Fig. 5), which could provide information on effective parameters of the model.

ACKNOWLEDGMENTS

The authors would like to thank D. F. Agterberg, I. Bonalde, E. Bauer, J. Goryo, Y. Kato, M. Matsumoto, M. Yogi, K. Izawa, and A. Koga for helpful discussions. One of us (N.H.) acknowledges support from the Japan Society for the Promotion of Science (2003 PFRA Program). The authors are also grateful for financial support from the Swiss Nationalfonds and the NCCR MaNEP.

APPENDIX

In this Appendix, we describe the procedure for deriving the quasiclassical Green functions for a noncentrosymmetric

superconductor with the Rashba-type spin-orbit coupling represented by Eqs. (1) and (2) and with the gap function of Eq. (3). The explicit form of the Eilenberger equations which will be given here [Eqs. (A10) and (A13)] would be useful for future studies in inhomogeneous systems such as surfaces, junctions, and vortices[24,53] in the noncentrosymmetric superconductor.

We start with the Eilenberger equation given in Eq. (5), namely[41]

$$i\partial\check{g} + [i\omega_n\check{\tau}_3 - \alpha\check{g}_k \cdot \check{\mathbf{S}} - \check{\Delta}, \check{g}] = 0, \tag{A1}$$

where we have defined $\partial = \mathbf{v}_F(s)\cdot\boldsymbol{\nabla}$. It is convenient to define, for the Green functions [Eq. (4)],

$$\hat{g} = \hat{g}_0, \quad \hat{f} = \hat{f}_0 i\hat{\sigma}_y, \quad \hat{\bar{f}} = -i\hat{\sigma}_y\hat{\bar{f}}_0, \quad \hat{\bar{g}} = -\hat{\sigma}_y\hat{\bar{g}}_0\hat{\sigma}_y. \tag{A2}$$

We also define, for the gap function [Eq. (3)],

$$\hat{\Delta} = \hat{\Delta}_0 i\hat{\sigma}_y, \quad \hat{\Delta}^\dagger = -i\hat{\sigma}_y\hat{\Delta}_0^\dagger, \tag{A3}$$

where

$$\hat{\Delta}_0(\mathbf{r}, \tilde{\mathbf{k}}) = \Psi(\mathbf{r})\hat{\sigma}_0 + \Delta(\mathbf{r})(-\tilde{k}_y\hat{\sigma}_x + \tilde{k}_x\hat{\sigma}_y). \tag{A4}$$

The Eilenberger equation (A1) is then written down to

$$\partial\hat{g}_0 + i\alpha\mathbf{g}_k\cdot(\hat{\boldsymbol{\sigma}}\hat{g}_0 - \hat{g}_0\hat{\boldsymbol{\sigma}}) + (\hat{\Delta}_0\hat{\bar{f}}_0 - \hat{f}_0\hat{\Delta}_0^\dagger) = 0, \tag{A5a}$$

$$(\partial + 2\omega_n)\hat{f}_0 + i\alpha\mathbf{g}_k\cdot(\hat{\boldsymbol{\sigma}}\hat{f}_0 - \hat{f}_0\hat{\boldsymbol{\sigma}}) + (\hat{\Delta}_0\hat{\bar{g}}_0 - \hat{g}_0\hat{\Delta}_0) = 0, \tag{A5b}$$

$$(\partial - 2\omega_n)\hat{\bar{f}}_0 + i\alpha\mathbf{g}_k\cdot(\hat{\boldsymbol{\sigma}}\hat{\bar{f}}_0 - \hat{\bar{f}}_0\hat{\boldsymbol{\sigma}}) + (\hat{\Delta}_0^\dagger\hat{g}_0 - \hat{\bar{g}}_0\hat{\Delta}_0^\dagger) = 0, \tag{A5c}$$

$$\partial\hat{\bar{g}}_0 + i\alpha\mathbf{g}_k\cdot(\hat{\boldsymbol{\sigma}}\hat{\bar{g}}_0 - \hat{\bar{g}}_0\hat{\boldsymbol{\sigma}}) + (\hat{\Delta}_0^\dagger\hat{f}_0 - \hat{\bar{f}}_0\hat{\Delta}_0) = 0, \tag{A5d}$$

where $\mathbf{g}_k = \sqrt{3/2}(-\tilde{k}_y, \tilde{k}_x, 0)$.

From Eq. (11), the normalization conditions are

$$\hat{g}_0^2 + \hat{f}_0\hat{\bar{f}}_0 = \hat{\sigma}_0, \tag{A6a}$$

$$\hat{\bar{g}}_0^2 + \hat{\bar{f}}_0\hat{f}_0 = \hat{\sigma}_0, \tag{A6b}$$

$$\hat{g}_0\hat{f}_0 = -\hat{f}_0\hat{\bar{g}}_0, \tag{A6c}$$

$$\hat{\bar{g}}_0\hat{\bar{f}}_0 = -\hat{\bar{f}}_0\hat{g}_0. \tag{A6d}$$

Now, we consider a rotation in the spin space which is represented by the matrices ($\hat{U}_k^\dagger\hat{U}_k = \hat{U}_k\hat{U}_k^\dagger = \hat{\sigma}_0$),[29,32]

$$\hat{U}_k = \frac{1}{\sqrt{2}}\begin{pmatrix} 1 & -\bar{k}'_+ \\ \bar{k}'_- & 1 \end{pmatrix}, \quad \hat{U}_k^\dagger = \frac{1}{\sqrt{2}}\begin{pmatrix} 1 & \bar{k}'_+ \\ -\bar{k}'_- & 1 \end{pmatrix}, \tag{A7}$$

where $\bar{\mathbf{k}} = (\bar{k}_x, \bar{k}_y, 0) = (\cos\phi, \sin\phi, 0)$ and $\bar{k}'_\pm = \bar{k}_y \pm i\bar{k}_x$. A physical meaning of this rotation is that after the rotation the quantization axis in the spin space becomes parallel to the vector $\mathbf{g}_k \| (-\tilde{k}_y, \tilde{k}_x, 0)$ at each position on the Fermi surface.[10,29,54] We define the matrix elements of the Green functions after the rotation as

$$\hat{U}_k^\dagger\hat{g}_0\hat{U}_k = \begin{pmatrix} g_a & g_b \\ g_c & g_d \end{pmatrix}, \quad \hat{U}_k^\dagger\hat{f}_0\hat{U}_k = \begin{pmatrix} f_a & f_b \\ f_c & f_d \end{pmatrix},$$

$$\hat{U}_k^\dagger\hat{\bar{f}}_0\hat{U}_k = \begin{pmatrix} \bar{f}_a & \bar{f}_b \\ \bar{f}_c & \bar{f}_d \end{pmatrix}, \quad \hat{U}_k^\dagger\hat{\bar{g}}_0\hat{U}_k = \begin{pmatrix} \bar{g}_a & \bar{g}_b \\ \bar{g}_c & \bar{g}_d \end{pmatrix}. \tag{A8}$$

We apply $\hat{U}_k^\dagger$ and $\hat{U}_k$ to the Eilenberger equations (A5) from left and right respectively, so that we obtain the following sets of equations in the case when $\mathbf{g}_k$ and $\hat{\Delta}_0$ are given in Eqs. (9) and (A4). Here, we define $\alpha' = \alpha\sqrt{3/2}$ and

$$\Delta_I = \Psi + \Delta\sin\theta, \quad \Delta_{II} = \Psi - \Delta\sin\theta. \tag{A9}$$

For the Green functions with the suffix a,

$$\partial g_a + \Delta_{II}\bar{f}_a - \Delta_{II}^* f_a = 0, \tag{A10a}$$

$$(\partial + 2\omega_n)f_a + \Delta_{II}\bar{g}_a - \Delta_{II}g_a = 0, \tag{A10b}$$

$$(\partial - 2\omega_n)\bar{f}_a + \Delta_{II}^* g_a - \Delta_{II}^*\bar{g}_a = 0, \tag{A10c}$$

$$\partial\bar{g}_a + \Delta_{II}^* f_a - \Delta_{II}\bar{f}_a = 0. \tag{A10d}$$

For the b,

$$\partial g_b - 2i\alpha'\sin\theta g_b + \Delta_{II}\bar{f}_b - \Delta_I^* f_b = 0, \tag{A11a}$$

$$(\partial + 2\omega_n)f_b - 2i\alpha'\sin\theta f_b + \Delta_{II}\bar{g}_b - \Delta_I g_b = 0, \tag{A11b}$$

$$(\partial - 2\omega_n)\bar{f}_b - 2i\alpha'\sin\theta\bar{f}_b + \Delta_{II}^* g_b - \Delta_I^*\bar{g}_b = 0, \tag{A11c}$$

$$\partial\bar{g}_b - 2i\alpha'\sin\theta\bar{g}_b + \Delta_{II}^* f_b - \Delta_I\bar{f}_b = 0. \tag{A11d}$$

For the c,

$$\partial g_c + 2i\alpha'\sin\theta g_c + \Delta_I\bar{f}_c - \Delta_{II}^* f_c = 0, \tag{A12a}$$

$$(\partial + 2\omega_n)f_c + 2i\alpha'\sin\theta f_c + \Delta_I\bar{g}_c - \Delta_{II}g_c = 0, \tag{A12b}$$

$$(\partial - 2\omega_n)\bar{f}_c + 2i\alpha'\sin\theta\bar{f}_c + \Delta_I^* g_c - \Delta_{II}^*\bar{g}_c = 0, \tag{A12c}$$

$$\partial\bar{g}_c + 2i\alpha'\sin\theta\bar{g}_c + \Delta_I^* f_c - \Delta_{II}\bar{f}_c = 0. \tag{A12d}$$

For the d,

$$\partial g_d + \Delta_I\bar{f}_d - \Delta_I^* f_d = 0, \tag{A13a}$$

$$(\partial + 2\omega_n)f_d + \Delta_I\bar{g}_d - \Delta_I g_d = 0, \tag{A13b}$$

$$(\partial - 2\omega_n)\bar{f}_d + \Delta_I^*\bar{g}_d - \Delta_I^*\bar{g}_d = 0, \tag{A13c}$$

$$\partial \bar{g}_d + \Delta_{\rm I}^* f_d - \Delta_{\rm I} \bar{f}_d = 0. \tag{A13d}$$

Note above that the Green functions with the suffixes a, b, c, and d are decoupled from each other in these sets of the Eilenberger equations.

We can solve Eqs. (A11) and (A12) in the case of a spatially uniform system, and find that $g_b = f_b = \bar{f}_b = \bar{g}_b = 0$ and $g_c = f_c = \bar{f}_c = \bar{g}_c = 0$ for $\alpha' \neq 0$. We also notice that the Green functions with the suffixes b and c are zero everywhere (even if the order parameters $\Delta_{\rm I,II}$ are spatially inhomogeneous), when solving the differential equations (A11) and (A12) with the initial values equal to zero. On the other hand, the Green functions with the suffixes a and d in Eqs. (A10) and (A13) have finite values in general. Therefore, we can rewrite Eq. (A8) as

$$\hat{U}_k^\dagger \hat{g}_0 \hat{U}_k = \begin{pmatrix} g_a & 0 \\ 0 & g_d \end{pmatrix}, \quad \hat{U}_k^\dagger \hat{f}_0 \hat{U}_k = \begin{pmatrix} f_a & 0 \\ 0 & f_d \end{pmatrix},$$

$$\hat{U}_k^\dagger \hat{\bar{f}}_0 \hat{U}_k = \begin{pmatrix} \bar{f}_a & 0 \\ 0 & \bar{f}_d \end{pmatrix}, \quad \hat{U}_k^\dagger \hat{\bar{g}}_0 \hat{U}_k = \begin{pmatrix} \bar{g}_a & 0 \\ 0 & \bar{g}_d \end{pmatrix}. \tag{A14}$$

We obtain accordingly

$$\hat{g}_0 = \frac{1}{2} \begin{pmatrix} g_d + g_a & -\bar{k}'_+ (g_d - g_a) \\ -\bar{k}'_- (g_d - g_a) & g_d + g_a \end{pmatrix}, \tag{A15a}$$

$$\hat{f}_0 = \frac{1}{2} \begin{pmatrix} f_d + f_a & -\bar{k}'_+ (f_d - f_a) \\ -\bar{k}'_- (f_d - f_a) & f_d + f_a \end{pmatrix}, \tag{A15b}$$

$$\hat{\bar{f}}_0 = \frac{1}{2} \begin{pmatrix} \bar{f}_d + \bar{f}_a & -\bar{k}'_+ (\bar{f}_d - \bar{f}_a) \\ -\bar{k}'_- (\bar{f}_d - \bar{f}_a) & \bar{f}_d + \bar{f}_a \end{pmatrix}, \tag{A15c}$$

$$\hat{\bar{g}}_0 = \frac{1}{2} \begin{pmatrix} \bar{g}_d + \bar{g}_a & -\bar{k}'_+ (\bar{g}_d - \bar{g}_a) \\ -\bar{k}'_- (\bar{g}_d - \bar{g}_a) & \bar{g}_d + \bar{g}_a \end{pmatrix}, \tag{A15d}$$

and finally, from Eq. (A2),

$$\hat{g} = g_{\rm I} \hat{\sigma}_{\rm I} + g_{\rm II} \hat{\sigma}_{\rm II}, \tag{A16a}$$

$$\hat{f} = (f_{\rm I} \hat{\sigma}_{\rm I} + f_{\rm II} \hat{\sigma}_{\rm II}) i \hat{\sigma}_y, \tag{A16b}$$

$$\hat{\bar{f}} = -i \hat{\sigma}_y (\bar{f}_{\rm I} \hat{\sigma}_{\rm I} + \bar{f}_{\rm II} \hat{\sigma}_{\rm II}), \tag{A16c}$$

$$\hat{\bar{g}} = -\hat{\sigma}_y (\bar{g}_{\rm I} \hat{\sigma}_{\rm I} + \bar{g}_{\rm II} \hat{\sigma}_{\rm II}) \hat{\sigma}_y, \tag{A16d}$$

with

$$\hat{\sigma}_{\rm I,II} = \frac{1}{2} (\hat{\sigma}_0 \pm \bar{\mathbf{g}}_k \cdot \hat{\boldsymbol{\sigma}}), \quad \bar{\mathbf{g}}_k = (-\bar{k}_y, \bar{k}_x, 0). \tag{A17}$$

Here, we have defined $A_{\rm I} \equiv A_d$ and $A_{\rm II} \equiv A_a$, $(A = \{g, f, \bar{f}, \bar{g}\})$.

In the case of spatially uniform system, we obtain from the Eilenberger equations (A10) and (A13) and the normalization conditions in Eq. (A6),

$$g_{\rm I} \equiv g_d = \frac{\omega_n}{B_{\rm I}}, \quad g_{\rm II} \equiv g_a = \frac{\omega_n}{B_{\rm II}}, \tag{A18a}$$

$$f_{\rm I} \equiv f_d = \frac{\Delta_{\rm I}}{B_{\rm I}}, \quad f_{\rm II} \equiv f_a = \frac{\Delta_{\rm II}}{B_{\rm II}}, \tag{A18b}$$

$$\bar{f}_{\rm I} \equiv \bar{f}_d = \frac{\Delta_{\rm I}^*}{B_{\rm I}}, \quad \bar{f}_{\rm II} \equiv \bar{f}_a = \frac{\Delta_{\rm II}^*}{B_{\rm II}}, \tag{A18c}$$

$$\bar{g}_{\rm I} \equiv \bar{g}_d = \frac{-\omega_n}{B_{\rm I}}, \quad \bar{g}_{\rm II} \equiv \bar{g}_a = \frac{-\omega_n}{B_{\rm II}}, \tag{A18d}$$

with

$$B_{\rm I,II} = \sqrt{\omega_n^2 + |\Delta_{\rm I,II}|^2}. \tag{A19}$$

At last, in these equations we replace $\omega_n \to \omega_n + q$ comparing Eq. (15) with Eq. (A1), so that we obtain the Green functions in Eqs. (21).

[1] V. M. Edelstein, Phys. Rev. Lett. **75**, 2004 (1995).

[2] L. P. Gor'kov and E. I. Rashba, Phys. Rev. Lett. **87**, 037004 (2001).

[3] P. A. Frigeri, D. F. Agterberg, A. Koga, and M. Sigrist, Phys. Rev. Lett. **92**, 097001 (2004); *ibid.* **93**, 099903(E) (2004).

[4] K. V. Samokhin, E. S. Zijlstra, and S. K. Bose, Phys. Rev. B **69**, 094514 (2004); *ibid.* **70**, 069902(E) (2004).

[5] I. A. Sergienko and S. H. Curnoe, Phys. Rev. B **70**, 214510 (2004).

[6] I. A. Sergienko, Physica B **359–361**, 581 (2005).

[7] E. Bauer, G. Hilscher, H. Michor, Ch. Paul, E. W. Scheidt, A. Gribanov, Yu. Seropegin, H. Noël, M. Sigrist, and P. Rogl, Phys. Rev. Lett. **92**, 027003 (2004).

[8] E. Bauer, G. Hilscher, H. Michor, M. Sieberer, E. W. Scheidt, A. Gribanov, Yu. Seropegin, P. Rogl, A. Amato, W. Y. Song, J.-G. Park, D. T. Adroja, M. Nicklas, G. Sparn, M. Yogi, and Y. Kitaoka, Physica B **359–361**, 360 (2005).

[9] E. Bauer, G. Hilscher, H. Michor, M. Sieberer, E. W. Scheidt, A. Gribanov, Yu. Seropegin, P. Rogl, W. Y. Song, J.-G. Park, D. T. Adroja, A. Amato, M. Nicklas, G. Sparn, M. Yogi, and Y. Kitaoka, Czech. J. Phys. **54**, D401 (2004).

[10] E. Bauer, I. Bonalde, and M. Sigrist, Fiz. Nizk. Temp. **31**, 984 (2005) [Low Temp. Phys. **31**, 748 (2005)].

[11] G. Dresselhaus, Phys. Rev. **100**, 580 (1955).

[12] E. I. Rashba, Fiz. Tverd. Tela (Leningrad) **1**, 407 (1959) [Sov. Phys. Solid State **1**, 368 (1959)].

[13] T. Yasuda, H. Shishido, T. Ueda, S. Hashimoto, R. Settai, T. Takeuchi, T. D. Matsuda, Y. Haga, and Y. Onuki, J. Phys. Soc.

Jpn. **73**, 1657 (2004).
[14] M. Yogi, Y. Kitaoka, S. Hashimoto, T. Yasuda, R. Settai, T. D. Matsuda, Y. Haga, Y. Onuki, P. Rogl, and E. Bauer, Phys. Rev. Lett. **93**, 027003 (2004).
[15] M. Yogi, Y. Kitaoka, S. Hashimoto, T. Yasuda, R. Settai, T. D. Matsuda, Y. Haga, Y. Onuki, P. Rogl, and E. Bauer, Physica B **359–361**, 389 (2005).
[16] M. Yogi, Y. Kitaoka, S. Hashimoto, T. Yasuda, R. Settai, T. D. Matsuda, Y. Haga, Y. Onuki, P. Rogl, and E. Bauer, J. Phys. Chem. Solids (to be published).
[17] K. Ueda, K. Hamamoto, T. Kohara, G. Motoyama, and Y. Oda, Physica B **359–361**, 374 (2005).
[18] K. Izawa, Y. Kasahara, Y. Matsuda, K. Behnia, T. Yasuda, R. Settai, and Y. Onuki, Phys. Rev. Lett. **94**, 197002 (2005); K. Maki, D. Parker, and H. Won, cond-mat/0508429 (unpublished).
[19] I. Bonalde, W. Brämer-Escamilla, and E. Bauer, Phys. Rev. Lett. **94**, 207002 (2005).
[20] N. Metoki, K. Kaneko, T. D. Matsuda, A. Galatanu, T. Takeuchi, S. Hashimoto, T. Ueda, R. Settai, Y. Onuki, and N. Bernhoeft, J. Phys.: Condens. Matter **16**, L207 (2004); Physica B **359–361**, 383 (2005).
[21] A. Amato, E. Bauer, and C. Baines, Phys. Rev. B **71**, 092501 (2005).
[22] M. Ishikawa, S. Yamashita, Y. Nakazawa, N. Wada, and N. Takeda, J. Phys.: Condens. Matter **17**, L231 (2005); M. Ishikawa and N. Takeda, Solid State Commun. **133**, 249 (2005).
[23] N. Hayashi, K. Wakabayashi, P. A. Frigeri, and M. Sigrist, cond-mat/0504176 (unpublished).
[24] N. Hayashi, K. Wakabayashi, P. A. Frigeri, Y. Kato, and M. Sigrist, cond-mat/0510547 (unpublished).
[25] From another approach, the NMR relaxation rate in noncentrosymmetric superconductors is theoretically discussed in, K. V. Samokhin, Phys. Rev. B **72**, 054514 (2005); see also S. Fujimoto, Ref. 32.
[26] P. A. Frigeri, D. F. Agterberg, and M. Sigrist, New J. Phys. **6**, 115 (2004).
[27] P. A. Frigeri, D. F. Agterberg, A. Koga, and M. Sigrist, Physica B **359–361**, 371 (2005).
[28] R. P. Kaur, D. F. Agterberg, and M. Sigrist, Phys. Rev. Lett. **94**, 137002 (2005).
[29] P. A. Frigeri, D. F. Agterberg, I. Milat, and M. Sigrist, cond-mat/0505108 (unpublished).
[30] P. W. Anderson, Phys. Rev. B **30**, 4000 (1984).
[31] One may choose a more complicated spin-triplet state with $\mathbf{d}_k \| \mathbf{g}_k$, for example $\mathbf{d}_k = \Delta(1+\cos 2\theta)(-\tilde{k}_y, \tilde{k}_x, 0)$. However, in this paper we consider the simplest one, $\mathbf{d}_k = \Delta(-\tilde{k}_y, \tilde{k}_x, 0)$, for clarity.
[32] S. Fujimoto, Phys. Rev. B **72**, 024515 (2005).
[33] I. A. Sergienko, Phys. Rev. B **69**, 174502 (2004).
[34] G. Eilenberger, Z. Phys. **214**, 195 (1968).
[35] A. I. Larkin and Yu. N. Ovchinnikov, Zh. Eksp. Teor. Fiz. **55**, 2262 (1968) [Sov. Phys. JETP **28**, 1200 (1969)].
[36] J. W. Serene and D. Rainer, Phys. Rep. **101**, 221 (1983).
[37] N. Schopohl, J. Low Temp. Phys. **41**, 409 (1980).
[38] C. T. Rieck, K. Scharnberg, and N. Schopohl, J. Low Temp. Phys. **84**, 381 (1991).
[39] C. H. Choi and J. A. Sauls, Phys. Rev. B **48**, 13684 (1993).
[40] H. Kusunose, Phys. Rev. B **70**, 054509 (2004).
[41] In the beginning, in the Eilenberger equation in the general form of Eqs. (5) and (A1), we assume that the spin-orbit coupling α is sufficiently weak such that the spin-degeneracy lifting is small and the Fermi velocity v_F is constant with respect to the spin projections. Then, after finally reaching the physically relevant parts of the Eilenberger equation [Eqs. (A10) and (A13)] for the specific set of the spin-orbit coupling and the gap function [(2) and (3)], we can set $\alpha > T_c$ (even $\alpha \gg T_c$, but $\alpha \ll \varepsilon_F$) and relax the restriction on v_F because v_F in these Eqs. (A10) and (A13) are interpreted as two mutually independent Fermi velocities on the distinctly different Fermi surfaces split into I and II.
[42] C. H. Choi and P. Muzikar, Phys. Rev. B **36**, 54 (1987).
[43] C. H. Choi and P. Muzikar, Phys. Rev. B **37**, R5947 (1988).
[44] C. H. Choi and P. Muzikar, Phys. Rev. B **39**, 11296 (1989).
[45] G. Preosti and P. Muzikar, Phys. Rev. B **51**, R15634 (1995).
[46] C. H. Choi and P. Muzikar, in *Field Theories in Condensed Matter Physics: A Workshop*, edited by Z. Tesanovic (Addison-Wesley, Reading, MA, 1990), p. 51.
[47] V. P. Mineev, Int. J. Mod. Phys. B **18**, 2963 (2004).
[48] Comparing the notation of the spin-triplet order parameter (Δ) with that in Ref. 29 (*d*), we have the relation $\sin\theta = d|\mathbf{g}_k|/\Delta = |\mathbf{g}_k|\sqrt{2/3}$, ($\Delta = d\sqrt{3/2}$). Substituting this into Eqs. (26), (32), and (33), we can use these equations to calculate the superfluid density also for other noncentrosymmetric systems with general $\mathbf{g}_k$ (but $\langle \mathbf{g}_k^2 \rangle = 1$).
[49] In principle, the anisotropy (or deformation) of each split Fermi surface (due to, e.g., the antisymmetric spin-orbit coupling [Eq. (1)]) can be incorporated through $\mathbf{v}_F(s)$ and $N_F(s)$, namely through the $\tilde{\mathbf{k}}$ dependence of $\mathbf{v}_{I,II}$ in Eq. (26) and the forms of each Fermi-surface average $\langle \ldots \rangle$. However, the most important qualitative effect of those split Fermi surfaces characteristic of the noncentrosymmetric systems is that different superconducting gaps can appear on each Fermi surface. Thermodynamic properties at low T are determined predominantly by the gap topology (such as line-node, point-node, and full gaps).
[50] S. K. Yip, Phys. Rev. B **65**, 144508 (2002).
[51] S. Hashimoto, T. Yasuda, T. Kubo, H. Shishido, T. Ueda, R. Settai, T. D. Matsuda, Y. Haga, H. Harima, and Y. Onuki, J. Phys.: Condens. Matter **16**, L287 (2004); Y. Onuki, T. Yasuda, H. Shishido, S. Hashimoto, T. Ueda, R. Settai, T. D. Matsuda, Y. Haga, and H. Harima, Physica B **359–361**, 368 (2005).
[52] E.-W. Scheidt, F. Mayr, G. Eickerling, P. Rogl, and E. Bauer, J. Phys.: Condens. Matter **17**, L121 (2005); See also, J. S. Kim, D. J. Mixson, D. J. Burnette, T. Jones, P. Kumar, B. Andraka, G. R. Stewart, V. Craciun, W. Acree, H. Q. Yuan, D. Vandervelde, and M. B. Salamon, Phys. Rev. B **71**, 212505 (2005).
[53] N. Hayashi, Y. Kato, K. Wakabayashi, P. A. Frigeri, and M. Sigrist, cond-mat/0510548 (unpublished).
[54] S. S. Saxena and P. Monthoux, Nature **427**, 799 (2004).